Roles of Singlet Fission in the Photosensitization of Silicon Phthalocyanine

Tsuneda, Takao

Taketsugu, Tetsuya

Roles of Singlet Fission in the Photosensitization of Silicon Phthalocyanine

Takao Tsuneda[**,†,‡] and Tetsuya Taketsugu[†,¶]

†*Department of Chemistry, Faculty of Science, Hokkaido University, Sapporo 060-0810, Japan*

‡*Graduate School of Science Technology and Innovation, Kobe University, Nada-ku, Kobe, Hyogo 657-8501, Japan*

¶*Institute for Chemical Reaction Design and Discovery (WPI-ICReDD), Hokkaido University, Sapporo 001-0021, Japan*

E-mail: tsuneda@phoenix.kobe-u.ac.jp

Abstract

The roles of singlet fission in the triplet generation of silicon phthalocyanine (SiPc), a compound analogous to IRDye700DX photosensitizer used in near-infrared photoimmunotherapy, are investigated by considering the energetical relation between the excitations of this compound. These excitations are obtained through spin-flip long-range corrected time-dependent density functional theory calculations. To initiate singlet fission, chromophores must meet two conditions: 1. Near-degenerate low-lying singlet and quintet (triplet-triplet) excitations with a considerable energy gap of the lowest singlet and triplet excited states, and 2. Moderate π-stacking energy of chromophores, which is higher than but not far from the solvation energy, to facilitate the dissociation and generation of triplet-state chromophores. The present calculations demonstrate that SiPc satisfies both of these conditions after the formation of π-stacking irrespective of the presence of an axial ligand(s), suggesting that singlet fission plays a crucial role in the triplet generation process, although intersystem crossing occurs simultaneously at a very slow rate.

Graphical TOC Entry

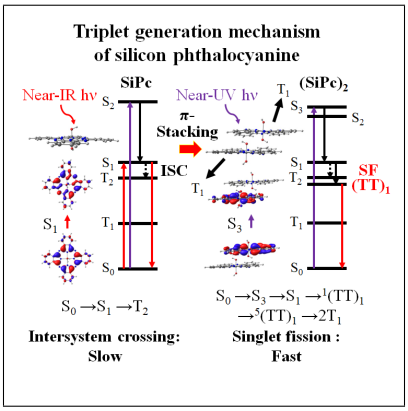

Phthalocyanine complexes serve as photosensitizers and find applications in a wide range of fields, including photovoltaics, photouncaging techniques, optoelectronics, photocatalysis, and photoimmunotherapy.[1,2] In particular, silicon phthalocyanine (SiPc) is a widely utilized and versatile representative phthalocyanine complex, finding extensive applications in organic photovoltaics,[3–5] organic light-emitting diodes,[6,7] organic photodetectors,[8] and other devices. Notably, SiPc stands out as the most commonly employed photosensitizer in near-infrared photoimmunotherapy.[9] Due to their high aggregatability, phthalocyanine complexes exhibit low solubility in common solvents. In the case of SiPc, aggregation into dimers results in a shift of the fluorescence to lower energy by approximately 4000 cm^{-1}, accompanied by a substantial reduction in emission quantum yield, by a factor of 10^{-3}.[10] This decrease in quantum yield following dimerization is attributed to rapid nonradiative decay.[10] Conversely, the peak absorption shifts to higher energy by about 1000 cm^{-1}.[11] Although significant changes in the electronic state of SiPc have been reported after dimerization, a detailed mechanistic explanation remains elusive.

In the context of photosensitization, our recent studies focused on elucidating the triplet generation mechanisms of four prominent organic photosensitizers: benzophenone, borondipyrromethene (BODIPY), methylene blue, and rose bengal.[12] Notably, it has been observed that many organic photosensitizers generate triplet states more rapidly than they undergo deexcitation to the ground states, despite the expectation of weak spin-orbit couplings due to their heavy atom-free structures. We, therefore, explored the contribution of singlet fission (SF) to the triplet generation mechanisms. Our particular emphasis was on understanding the influence of π-stacking on the electronic states of these photosensitizers concerning singlet, triplet, and quintet (triplet-triplet) state energies. In our previous study, we had revealed that SF in a BODIPY derivative proceeds through π-stacking.[13] As a result, we have determined that the quintet states are energetically lower and closely aligned with the lowest singlet states for these photosensitizers. This implies that SF likely plays a significant role in the triplet generation of these photosensitizers through π-stacking, while

intersystem crossings occur at a comparatively slower rate. This suggests that SF may also contribute to the triplet generation of SiPc.

SF is a process that involves the conversion of singlet states (S_n, $n \geq 1$) into quintet triplet-triplet (TT) excited states, where TT signifies two distinct triplet T states, occurring through a spin-allowed transition. Subsequently, the spin-forbidden transition proceeds from singlet ^{1}(TT) to quintet ^{5}(TT) excited states[14–16] through the zero-field splitting interaction and the subsequent re-encounter,[17] ultimately splitting the quintet ^{5}(TT) state into two T states if it does not decay to the ground state:

$$S_0 + S_n \rightarrow {}^1(\mathrm{TT}) \rightarrow {}^5(\mathrm{TT}) \rightarrow 2\mathrm{T}. \tag{1}$$

SF occurs when the triplet excitation energy is slightly less than half of the singlet excitation energy:[14,18]

$$(\mathrm{TT}) \sim 2\Delta E(\mathrm{T}) \lesssim \Delta E(S_n), \tag{2}$$

where ΔE is the excitation energy. Theoretically, near-degenerate energies are reported for the singlet and quintet (TT) states of π-stacking chromophores with only about 10 meV for tetracene dimer,[19] indicating that the ^{5}(TT) excitations are available to discuss the ^{1}(TT) excitations of SF processes. The concentration of chromophores significantly also affects the probability of SF due to the re-encounter requirement in the (TT) states.[20] Considering these findings, we proposed the conditions for SF as follows:[12] 1. Near-degenerate low-lying singlet and quintet (triplet-triplet) excitations with a considerable S_1-T_1 energy gap, and 2. A moderate π-stacking energy of chromophores, which is higher than but not far from the solvation energy, facilitates the dissociation and generation of triplet-state chromophores. By confirming if SiPc satisfies these conditions similar to other photosensitizers, we can explore the triplet generation mechanism of this molecule.

In this study, we investigate the excited states of SiPc, varying between two, one, and

zero axial ligands, which is analogous to IRDye700DX dye in near-infrared photoimmunotherapy,[9,21] in the π-stacking structures to determine if the above-mentioned conditions for SF are met. The spin-flip long-range corrected (LC) time-dependent density functional theory (TDDFT) calculations are performed for this study, because the double excitation effects are known to play a crucial role in the excited states of photosensitizers.[12,22] Based on the calculated results, we propose the triplet generation mechanism of SiPc.

The excited state calculations of SiPc, featuring two, one, and zero axial ligands as shown in Fig. 1, were conducted using collinear spin-flip time-dependent density functional theory (TDDFT)[23,24] with the long-range correction (LC).[25,26] The LC-BLYP functional, which

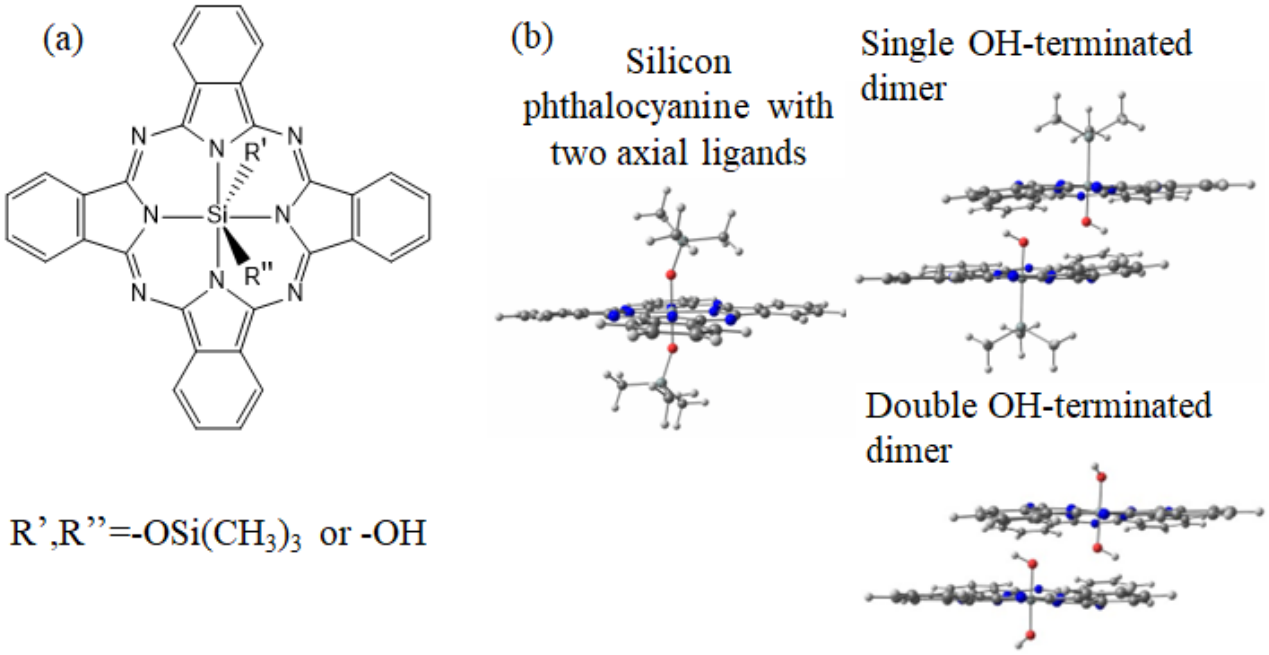

Figure 1: (a) The calculated structure of SiPc, with the axial ligand represented as a trimethylsiloxy group, mimicking IRDye700DX in near-infrared photoimmunotherapy. Following near-infrared (NIR) irradiation, the axial ligand undergoes cleavage, and a hydroxyl group replaces it. (b) Optimized structures of SiPc for the monomer, and the single and double OH-terminated ones for the π-stacking dimers. The Cartesian coordinates of these structures are compiled in Table S1 of the supporting information.

combines Becke 1988 exchange[27] with Lee-Yang-Parr correlation,[28] was employed along with the cc-pVTZ basis set.[29] The computational model was based on a structure resembling IRDye700DX used in near-infrared photoimmunotherapy, with the axial ligands initially set

as trimethylsiloxy groups before being substituted with OH groups. The conductor-like polarizable continuum model (CPCM)[30] for the solvent effect of water was applied to the ground state as a nonequilibrium solvent effect on the ground state. For the geometry optimizations of SiPc, the ωB97XD dispersion-corrected LC-DFT calculations were performed on the ground states with the same basis set. (the Cartesian coordinates of the optimized π-stacking structures are compiled in Table S1 of the supporting information.) A few initial structures were examined for the π-stacking dimers. The optimized structures for both the monomers and π-stacking dimers are depicted in Fig. 1(b). Additionally, TDDFT calculations of the ωB97XD functional (TDωB97XD) were compared. It is important to note that spin-flip LC-TDDFT has been confirmed to accurately predict excitation energies with or without double excitation effects,[31,32] making it the first time TDDFT could achieve this level of accuracy. In contrast, conventional TDDFT methods underestimate triplet excitation energies and overestimate singlet excitation energies for photosensitizers.[22] All LC-DFT and LC-TDDFT calculations were performed using the Gaussian 16 Revision A.03 program,[33] while spin-flip LC-TDDFT calculations were conducted using the development version of the GAMESS program.[34]

Let us begin by examining the electronic excitations of SiPc before the axial ligand substitution, where both R' and R" are trimethylsiloxyl groups -OSi$(CH_3)_3$ as shown in Fig. 1(a). Table 1 summarizes the excitation energies for T_1, T_2, S_1 and S_2 excitations along with the main transitions. The triplet excitation energies of SiPc, calculated using TDωB97XD,

Table 1: Calculated lowest-lying vertical excitation energies (eV) of SiPc by spin-flip LC-TDBLYP with cc-pVTZ basis set and CPCM solvent effect of water. The corresponding excitation energies of TDωB97XD are also listed with the oscillator strength (f) for comparison. Main transitions of spin-flip LC-TDBLYP excitations are also shown with the coefficients of the response functions in parentheses, in which the notations H and L indicate HOMO and LUMO. The experimental main peak is observed at 1.80 eV (690nm).[35]

State	Spin-flip LC-TDBLYP			TDωB97XD			
	eV	nm	Main transitions	No.	eV	nm	f
S_0	0	-	Ground (0.960) αH,βH→αL,βL+1 (−0.195)		0	-	–
T_1	0.61	2020			0.94	1315	–
T_2	1.18	1050	βH→ βL+1 (0.719) αH→αL (0.646)	-	-	-	-
S_1	1.53 (−0.27)	810 (120)	βH→ βL (−0.909) αH−3→αL (0.234)	1	1.89	655	0.5575
S_2	2.72	456	αH→αL (0.716) βH→ βL+1 (0.638)	2	1.90	654	0.5571

are compiled for comparison in Table S2. Notably, all three lowest-lying excitations involve a HOMO→LUMO transition as the primary transition. Interestingly, a new singlet excitation (S_1) is observed in this model, which is not present in the TDωB97XD calculation. As this S_1 excited state lies below the main peak of the UV-Vis spectrum at 1.80 eV (690 nm), its long lifetime supports the possibility of ISC in SiPc, consistent with the negligible peak in the spectrum. However, it is crucial to note that there is a small energy difference between the S_1 and T_2 excitation energies (0.35 eV), suggesting the possibility of an ISC process. The molecular orbital images of the main transitions for the lowest-lying excitations of SiPc are illustrated in Fig. 2. The figure reveals that the S_1 excitation mainly involves a $\pi\pi^*$

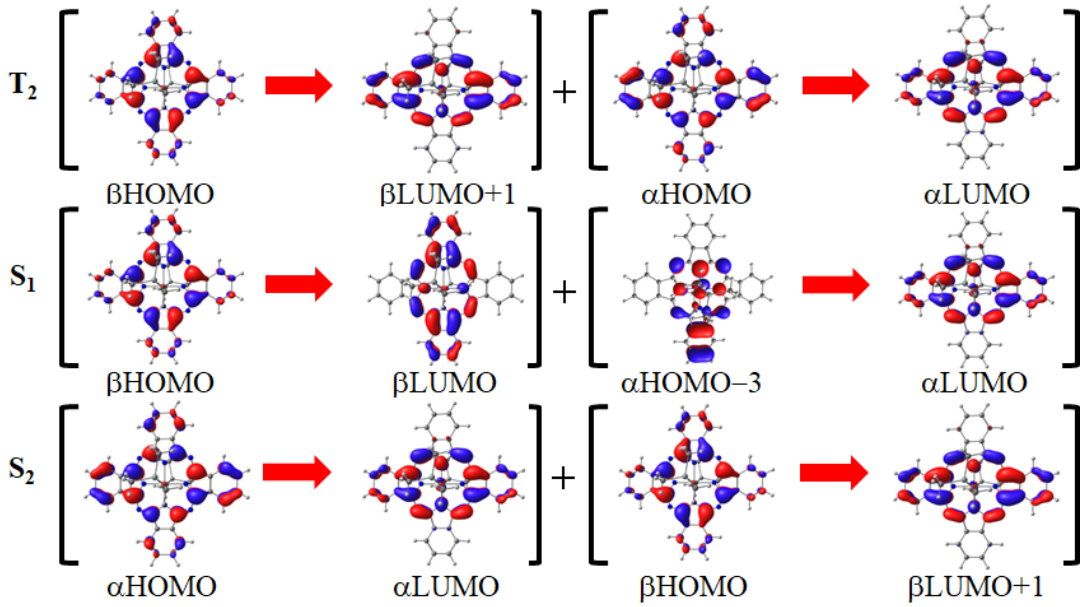

Figure 2: Images of the molecular orbitals illustrating the main transitions of the three lowest-lying singlet excitations of SiPc. The transitions of the excitations are determined using spin-flip LC-TDBLYP/cc-pVTZ calculations, while the molecular orbital images are obtained using LC-BLYP/cc-pVTZ calculations. The CPCM model of water is considered for the solvent model.

transition from two benzene rings to the central part of the phthalocyanine ring, while the T_2 excitation slightly contains an $n\pi^*$ transition to the n orbitals of N atoms beside this $\pi\pi^*$ transition in both of the two main transitions. According to the El-Sayed rule,[36,37] which establishes that spin-orbit couplings are significant only for transitions between orbitals with different angular momenta, such as $n\pi^*$ excitations,[37] ISC from the S_1 to the T_2 excitations is indicated to proceed, albeit slowly. This result aligns with the experimental finding of a very small ISC rate for IRDye700DX containing silicon phthalocyanine (0.019 ± 0.002).[38] Additionally, it is worth noting that SF does not occur for SiPc when the axial ligands are bound to both sides of SiPc as shown in Fig. 1(a). If the axial ligands are bulky, they prevent the formation of π-stacking between the phthalocyanine rings. This explains why the slow progression of triplet generations in SiPc proceed through ISC until the bulky axial ligands are cleaved.

Next, we performed excitation energy calculations for the single OH-terminated SiPc, which replaces one axial ligand with an OH group, as shown in Fig. 1(b). Unlike SiPc with two axial ligands, this molecule can form the π-stacking dimer, although dimerization is constrained due to the bond with the axial ligand on the other side. Table 2 summarizes the calculated excitation energies of the lowest-lying singlet excitations of the single OH-terminated SiPc and the main transitions of these excitations for the monomer and π-stacking dimer. As shown in the table, the three lowest-lying excitations, which involve the HOMO→LUMO transition, exhibit similar excitation energies compared to those of SiPc with two axial ligands for the monomer. Therefore, this result suggests a small ISC rate of the monomer for the single OH-terminated SiPc. For the π-stacking dimer, the excitations undergo drastic changes compared to those of the monomer. The T_3 and T_4 excitations, consisting of double excitations, appear in between S_1 and S_2 excitations. On the other hand, the T_2 and S_1 excitations appear to be similar to those of the monomer, although the T_2-S_1 energy gap decreases from 0.35 to 0.23 eV, indicating the faster ISC rate. The most notable difference in the excitations from those of the monomer is the presence of the quintet $^5(TT)_1$ excitation, which plays a main role in SF. The $^5(TT)_1$ excitation energy is just twice as large as the T_1 one in the ωB97XD calculation, estimated to be 1.20 eV, which is nearly degenerate and just below the T_2 excitation energy (1.24 eV) according to the spin-flip LC-TDBLYP results. The $^5(TT)_1$ excitation energy is 0.27 eV lower than the S_1 excitation energy. While this energy difference is significant for spin-forbidden singlet-triplet ISC processes, it is relatively small for the spin-allowed singlet-singlet deexcitations in initial SF processes. Considering that $^5(TT)_1$ excitation energies are usually close to the corresponding singlet $^1(TT)_1$ ones and the S_1 to $^1(TT)_1$ transition is spin-allowed, we expect the S_1 →$(TT)_1$ transition to rapidly proceed in the π-stacked single OH-terminated SiPc. However, it is crucial to note that the oscillator strength corresponding to the S_1 excitation is extremely small, unlike that of the monomer. This implies that $^1(TT)_1$ is not generated directly from the photoabsorption of the S_1 excitation. Upon examining the oscillator

strengths in Table 2, it is evident that photoabsorption in the dimer occurs for the S_3 and S_4 excitations. This is consistent with the experimental UV-Vis absorption spectrum, which exhibits a prominent absorption peak around 355 nm (3.49 eV). This indicates that the entrance to the SF process corresponds to the absorption around 355 nm, corresponding to the S_3 and S_4 excitations. Therefore, photoabsorption with an energy of 355 nm or higher is required for efficient SF to occur in the dimer. Once SF initiates, it is expected to generate triplet states much more rapidly than the ISC processes of the monomer.

Figure 3 illustrates the molecular orbital images of the main transitions for the lowest-lying excitations of the single OH-terminated SiPc. As shown in the figure, the main transitions of the three lowest-lying excitations are similar to those of the OH-unterminated SiPc for the monomer. The main difference is in the distribution to the outer benzene rings of αHOMO-3 involved in the S_1 excitation transition. However, the effect of this difference is expected to be minor, because it is not the main transition. Similar to the case of OH-unterminated SiPc, the transition in the T_2 excitation has a limited inclusion of $n\pi^*$. Therefore, according to the El-Sayed rule,[36,37] ISC is presumed to proceed very slowly. The figure also shows the molecular orbital images of the main transitions for the π-stacking dimer from the side views (for the images from the top views, see Fig. S1 of the supporting information). The figure indicates that though the T_2 and S_1 excitations both contain intermolecular charge transfers. What we should note is that both of these excitations partially involve an $n\pi^*$ transition in the main transition. According to the El-Sayed rule, which establishes a significant ISC rate between $\pi\pi^*$ and $n\pi^*$ excitations, this finding indicates a small ISC rate in the dimer. SF proceeds independently of the nature of the singlet and triplet excitations. Instead, it requires moderate π-stacking energy to form and dissociate the π-stacking dimer at room temperature. The π-stacking energy of the single OH-terminated SiPc is calculated as 27.8 kcal/mol in the ωB97XD calculation. Since the solvation energy of the hydrophobic phthalocyanine surface is expected to be low, this energy is moderate enough to allow the SF process. Considering the above-mentioned close S_1 and

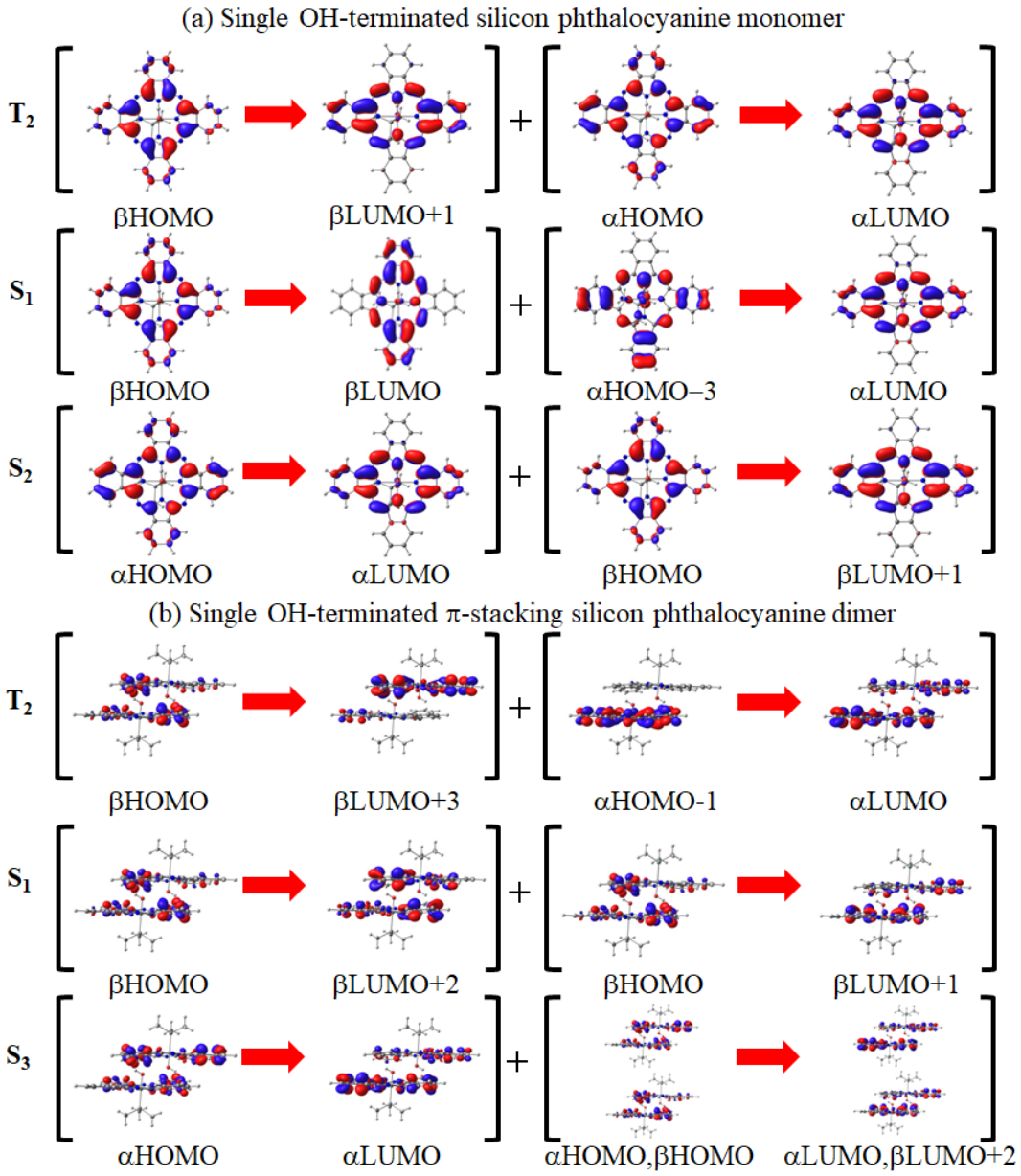

Figure 3: Images of the molecular orbitals depicting the main transitions of the three lowest-lying singlet excitations of the single OH-terminated SiPc for the monomer and π-stacking dimer. The transitions of the excitations are determined using spin-flip LC-TDBLYP/cc-pVTZ calculations, while the molecular orbital images are obtained using LC-BLYP/cc-pVTZ calculations. The CPCM model of water is considered for the solvent model.

$(TT)_1$ excitation energies, we can conclude that the single OH-terminated SiPc satisfies the conditions for initiating SF after forming the π-stacking dimer.

Finally, we conducted excitation energy calculations for the double OH-terminated SiPc, where both axial ligands are replaced with OH groups (i.e., R', R" = -OH in Fig. 1(b)). The π-stacking is expected to occur smoothly for this molecule due to the lack of constraints from axial ligands. Table 3 presents the calculated excitation energies of the lowest-lying singlet excitations of the double OH-terminated SiPc and the main transitions for the monomer and π-stacking dimer. For the monomer, although the same main transitions are observed, the T_2 excitation energy increases, and the S_1 excitation energy decreases compared to those of the single OH-terminated SiPc. This results in a decreased S_1-T_1 gap, suggesting a decrease in the ISC rate. For the π-stacking dimer, the excitation energies are nearly the same as those of the single OH-terminated SiPc, but they exhibit different main transitions as mentioned later. Similar to the excitations of the single OH-terminated dimer, the T_3 and T_4 excitations, which involve double excitations, also appear between the S_1 and S_2 excitations. The energy gap between the T_2 and S_1 excitations (0.25 eV) is slightly larger than that of the single OH-terminated dimer (0.23 eV), indicating a slightly slower ISC rate. The $^5(TT)_1$ excitation energy is calculated to be 1.18 eV, which is nearly degenerate with the T_2 excitation and 0.30 eV lower than the S_1 excitation energy (1.48 eV). This small $^1(TT)_1$-S_1 gap supports the rapid initiation of the spin-allowed SF process for the double OH-terminated SiPc.

Figure 4 displays the molecular orbital images of the main transitions for the lowest-lying excitations of the double OH-terminated SiPc, similar to those of the single OH-terminated one. The figure shows that, for the monomer, the molecular orbitals with a tilted axis of 45 degrees constitute the main transition, different from those of single OH-terminated SiPc. Regarding these molecular orbitals, it is evident that the T_2 excitation includes a partial transition to the $n\pi^*$ orbitals of N atoms, while the S_1 excitation is composed of a $\pi\pi^*$ orbital transition. Following the El-Sayed rule, it suggests that ISC proceeds slowly in the

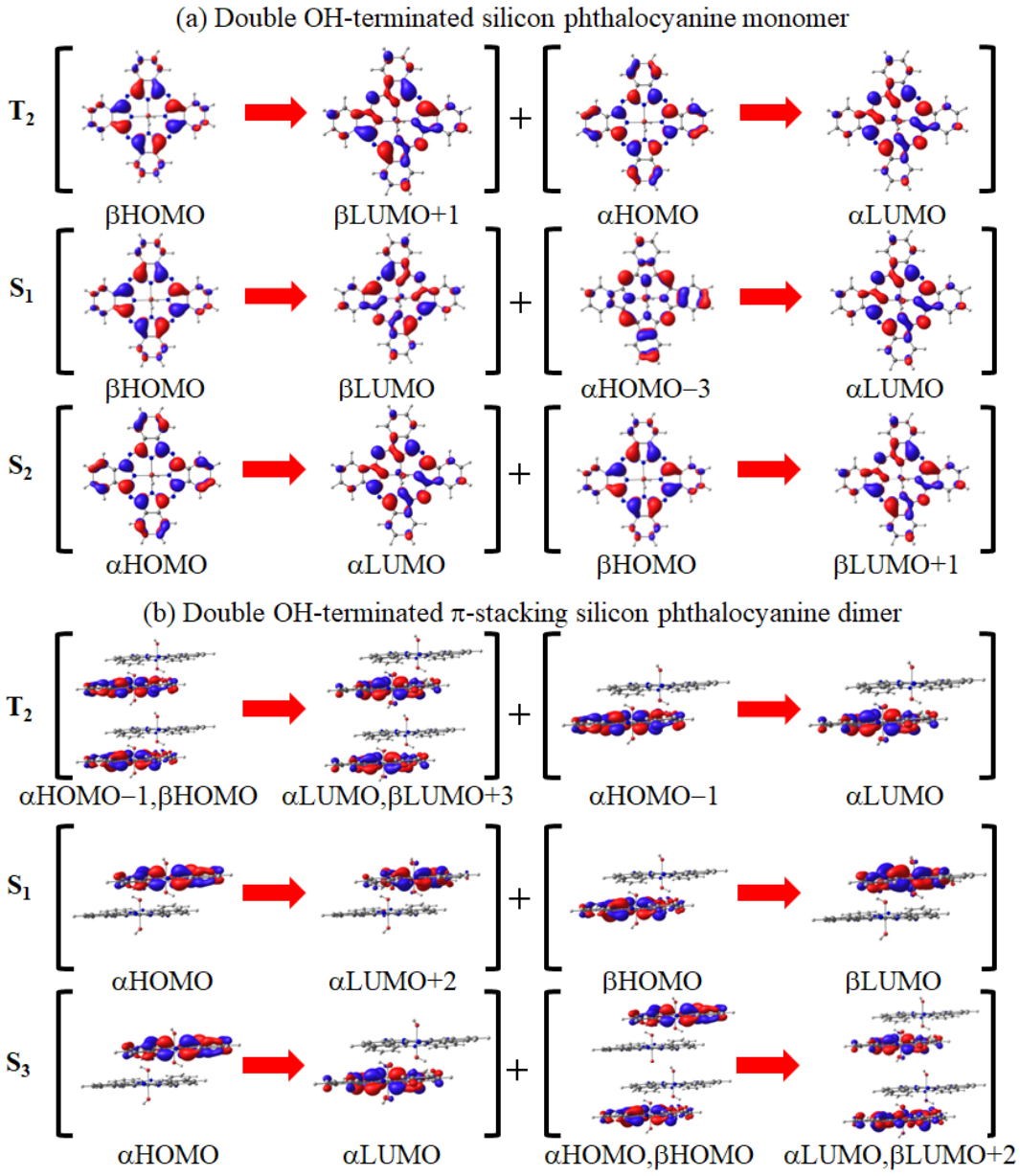

Figure 4: Images of the molecular orbitals illustrating the main transitions of the three lowest-lying singlet excitations of the double OH-terminated SiPc for the monomer and π-stacking dimer. The transitions of the excitations are determined using spin-flip LC-TDBLYP/cc-pVTZ calculations, while the molecular orbital images are obtained using LC-BLYP/cc-pVTZ calculations. The CPCM model of water is considered for the solvent model.

double OH-terminated SiPc, similar to the single OH-terminated SiPc. The molecular orbital images of the main transitions are also displayed for the π-stacking dimer from the side views (for the images from the top views, see Fig. S1 of the supporting information). As shown in the figure, the lowest-lying excitations of the π-stacking dimer consist of intramolecular excitations, in contrast to the excitations of the single OH-terminated SiPc. Upon examining the top views in Fig. S1, similar to the case of the monomer, the molecular orbitals of the main transition for the T_2 excitation include partial intramolecular $n\pi^*$ transitions, while intramolecular $\pi\pi^*$ transitions constitute those for the S_1 excitation. Therefore, following the El-Sayed rule, ISC in the dimer is expected to proceed slowly. As described above, the occurrence of SF necessitates a moderate π-stacking energy to facilitate the formation and dissociation of the π-stacking dimer at room temperature, irrespective of the characteristics of the singlet and triplet excitations. The π-stacking energy for the double OH-terminated SiPc is calculated to be 27.8 kcal/mol in the ωB97XD calculation. Therefore, considering the closely aligned S_1 and $(TT)_1$ excitation energies, the double OH-terminated SiPc meets the conditions for initiating SF. Following these results, it is suggested that SF and ISC simultaneously occur for the double OH-terminated SiPc, with the former process being faster than the latter.

Based on the above results, let us consider the shift in the fluorescence and absorption peaks due to the dimerization of SiPc, as mentioned above. Experiments show that the main fluorescence peak decreases by approximately 4000 cm^{-1} (=0.5 eV), and its emission quantum yield reduces to 10^{-3} due to the dimerization.[10] As clearly shown in Tables 2 and 3, these findings are attributed to the appearance of the low-energy $^1(TT)_1$ excitation and the dramatic decrease in the oscillator strength due to dimerization. According to these tables, the dimerization of SiPc results in the generation of (TT) excitations with energies 0.37 eV lower (single OH-terminated) or 0.24 eV lower (double OH-terminated) than the S_1 excitation of the monomer. In the case of the π-stacking dimer, the singlet (TT) excitation, which is the lowest singlet excitation reached upon de-excitation, emits fluorescence unless

it dissociates into two triplet states through the conversion to the quintet(TT) excitation. The calculated energy decrease is slightly lower than the experimental results, as the calculations do not account for the energy stabilization due to structural relaxation before the fluorescence of the ^{1}(TT) excitation, making it adiabatic fluorescence. Furthermore, the oscillator strength of the S_1 excitation dramatically decreases from 0.5861 to 0.0002 (single OH-terminated) or 0.6082 to 0.0000 (double OH-terminated) due to dimerization. Since the ^{1}(TT) excitation of SiPc has no absorption peak, the oscillator strength is considered extremely low. Therefore, the dramatic decrease in the quantum yield can also be explained by the computational results. It is also experimentally observed that the dimerization leads to an increase of approximately 1000 cm^{-1} (0.12 eV) in the absorption peak for a double OH-terminated dimer.[11] This small increase in excitation energy is due to the rise in S_1 excitation energy (0.06 eV) caused by dimerization. Though the oscillator strength for this excitation is calculated to be zero, we consider that it is not inherently zero due to the double excitation effects. The comparison with the above experiments confirms that the calculated electronic states after dimer formation are fundamentally consistent with the observations from the experiments. This strongly supports our conclusion that the triplet generation of SiPc proceeds by SF through the π-stacking dimerization.

Table 2: Calculated lowest-lying vertical excitation energies (eV) of single OH-terminated SiPc for the monomer (a) and π-stacking dimer (b) by spin-flip LC-TDBLYP with cc-pVTZ basis set and CPCM solvent effect of water. The corresponding excitation energies of TDωB97XD are also listed with the oscillator strength (f) for comparison. Main transitions of spin-flip LC-TDBLYP excitations, in which the notations H and L indicate HOMO and LUMO, are also shown with the coefficients of the response functions in parentheses. For the quintet $(TT)_1$ excitation, the excitation energy is calculated by ωB97XD. The experimental main peak is observed at 1.80 eV (690nm).[35] For the excitation energies, the errors from the main peak energy are attached for the corresponding S_2 excitation energies in parentheses. The presumed quintet (TT) excitation energy is also appended for the dimer in square brackets.

State	Spin-flip LC-TDBLYP			TDωB97XD			
	eV	nm	Main transitions	No.	eV	nm	f
(a) Monomer							
S_0	0	–	Ground (0.964) αH,βH→αL,βL+1 (−0.180)		0	–	–
T_1	0.61	2020			0.72	1728	–
T_2	1.19	1046	βH→ βL+1 (0.719) αH→αL (−0.647)	-	-	-	-
S_1	1.57 (−0.23)	791 (101)	βH→ βL (0.914) αH−3→αL (−0.222)	1	1.89	656	0.5861
S_2	2.74	453	αH→αL (−0.717) βH→ βL+1 (−0.640)	2	1.90	652	0.5790
(b) π-Stacking dimer							
S_0	0	–	Ground (−0.961) αH,βH→αL,βL+3 (−0.183)		0	–	–
T_1	0.60	2078			0.88	1407	–
$^5(TT)_1$	[1.20]	[1039]			1.76	705	–
T_2	1.24	999	βH→ βL+3 (−0.686) αH−1→αL (0.668)	-	-	-	-
S_1	1.47 (−0.33)	842 (152)	βH→ βL+2 (−0.879) βH→ βL+1 (−0.188)	1	1.75	708	0.0002
T_3	1.82	682	αH,βH→αL,βL (0.883) αH,βH→αL,βL+1 (−0.413)	–	–	–	–
T_4	2.10	592	αH,βH→αL,βL+1 (0.855) αH,βH→αL,βL (0.401)	–	–	–	–
S_2	2.49	498	βH→βL (−0.908) βH→ βL+1 (−0.338)	2	1.86	666	0.0009
S_3	2.55	485	αH→αL (−0.945) αH,βH→ αL,βL+2 (0.187)	3	1.92	644	0.8943
S_4	2.67	465	βH→βL+1 (0.945) βH→βL (−0.187)	4	1.96	632	0.9657

Table 3: Calculated lowest-lying vertical excitation energies (eV) of double OH-terminated SiPc for the monomer (a) and π-stacking dimer (b) by spin-flip LC-TDBLYP with cc-pVTZ basis set and CPCM solvent effect of water. The corresponding excitation energies of TDωB97XD are also listed with the oscillator strength (f) for comparison. Main transitions of spin-flip LC-TDBLYP excitations, in which the notations H and L indicate HOMO and LUMO, are also shown with the coefficients of the response functions in parentheses. For the quintet $(TT)_1$ excitation, the excitation energy is calculated by ωB97XD. The experimental main peak is observed at 1.80 eV (690nm).[35] For the excitation energies, the errors from the main peak energy are attached for the corresponding S_2 excitation energies in parentheses. The presumed quintet (TT) excitation energy is also appended for the dimer in square brackets.

State	Spin-flip LC-TDBLYP			TDωB97XD			
	eV	nm	Main transitions	No.	eV	nm	f
(a) Monomer							
S_0	0	–	Ground (0.964) αH,βH→αL,βL+1 (−0.180)		0	–	–
T_1	0.62	1995			0.76	1631	–
T_2	1.28	967	βH→ βL+1 (−0.690) αH→αL (0.678)	–	–	–	–
S_1	1.42 (−0.38)	873 (183)	βH→ βL (0.922) αH−3→αL (−0.278)	1	1.89	655	0.6082
S_2	2.79	445	αH→αL (−0.684) βH→ βL+1 (−0.670)	2	1.90	653	0.6069
(b) π-Stacking dimer							
S_0	0	–	Ground (−0.960) αH-1,βH→αL,βL+3 (−0.184)		0	–	–
T_1	0.59	2091			0.88	1401	–
$^5(TT)_1$	[1.18]	[1051]			1.76	703	–
T_2	1.23	1007	αH−1,βH→αL,βL+3 (−0.683) αH→αL (0.662)	–	–	–	–
S_1	1.48 (-0.32)	836 (146)	αH→αL+2 (0.922) βH→ βL (−0.278)	1	1.76	706	0.0000
T_3	1.82	683	αH,βH→αL,βL+1 (0.809) αH,βH→αL,βL (0.542)	–	–	–	–
T_4	2.10	592	αH,βH→αL,βL (−0.852) αH,βH→αL,βL+1 (0.406)	–	–	–	–
S_2	2.49	498	βH→βL (0.965) βH→ βL+2 (−0.168)	2	1.86	667	0.0009
S_3	2.56	484	αH→αL (0.951) αH,βH→ αL,βL+2 (−0.180)	3	1.92	644	0.8943
S_4	2.67	465	βH→βL+1 (0.945) βH→βL+2 (−0.122)	4	1.96	632	0.9657

Following the calculated results, the triplet generation mechanism of SiPc can be summarized in the following steps:

1. π-Stacking:

   SiPcs form a π-stacking structure on the OH-terminated sides. The π-stacked SiPcs show minimal oscillator strengths for the S_1 and S_2 excitations in the near-infrared region. Upon absorbing near-ultraviolet light around 355 nm (3.49 eV) or higher, they de-excite from the S_3 and S_4 or higher excited states, ultimately reaching the S_1 excited state.

2. Initiation of singlet fission:

   Singlet fission, then, initiates from the S_1 excited state for the π-stacked OH-terminated SiPc, generating the quintet $(TT)_1$ state. From this S_1 state, the intersystem crossing simultaneously occurs very slowly, leading to the formation of the T_1 state.

3. Triplet generation:

   The π-stacked SiPc dimer in the quintet $(TT)_1$ state splits into two SiPcs in the T_1 state. These generated T_1 states trigger the photosensitization, returning the process to step 2.

The schematic diagram of this mechanism is illustrated in Fig. 5.

In conclusion, we have examined the probabilities of singlet fission (SF) and intersystem crossing for silicon phthalocyanine (SiPc) considering the presence of axial ligand(s), through the π-stacking formation. To perform the excited state calculations, we employed spin-flip LC-TDDFT, which incorporates both long-range exchange and double excitation correlation effects to provide accurate excitation energies, including those related to charge transfers, for this photosensitizer. We have focused on elucidating the triplet generation mechanism through examination of excitation energies for singlet (S), triplet (T), and quintet triplet-triplet (TT) excitations. As a result, we have confirmed that SF is likely to be the main contributor to the triplet generation of SiPc after the formation of the π-stacking dimer

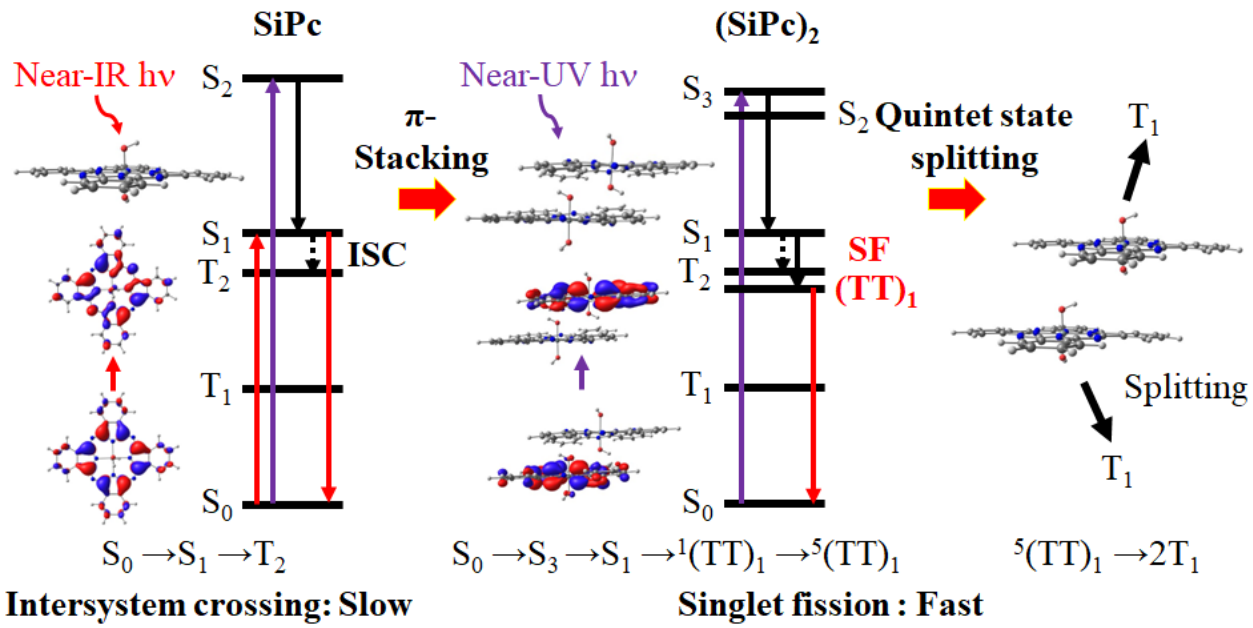

Figure 5: Schematic diagram depicting the triplet generation mechanism of SiPc.

irrespective of the presence of the axial ligand. This conclusion is supported by the anticipated slow intersystem crossing according to the El-Sayed rule, attributed to the small $n\pi^*$ character of the T_2 excitation, and the calculated small S_1-$(TT)_1$ gaps for both monomers and dimers. Note, however, that the SF progression starts not from the near-infrared absorption associated with the S_1 excitation but from the absorption in the near-ultraviolet regions, attributed to the S_3 and S_4 excitations, or higher-energy regions, The resulting triplet generation mechanism of SiPc presents a reasonable pathway for producing triplet states. Following these results, we anticipate that SF plays a significant role in the overall photochemistry of phthalocyanine complexes.

Acknowledgments

This research was financially supported by JST CREST, Japan (Grant No. JPMJCR1902).

Supporting Information Available

The Cartesian coordinates of the optimized structures of SiPc and its single and double OH-terminated ones are compiled in Table S1. In Table S2, the calculated triplet excitation energies of SiPcs are also shown. Figure S1 displays the top-view molecular orbital images of the main transitions of the lowest-lying singlet excitations of SiPcs.

Data availability

All data generated or analyzed during this study are included in this published article and its supplementary information files but are available from the corresponding author upon reasonable request.

Figure Captions

Fig. 1. (a) The calculated structure of SiPc, with the axial ligand represented as a trimethylsiloxy group, mimicking IRDye700DX in near-infrared photoimmunotherapy. Following near-infrared (NIR) irradiation, the axial ligand undergoes cleavage, and a hydroxyl group replaces it. (b) Optimized structures of SiPc for the monomer, and the single and double OH-terminated ones for the π-stacking dimers. The Cartesian coordinates of these structures are compiled in Table S1 of the supporting information.

Fig. 2. Images of the molecular orbitals illustrating the main transitions of the three lowest-lying singlet excitations of SiPc. The transitions of the excitations are determined using spin-flip LC-TDBLYP/cc-pVTZ calculations, while the molecular orbital images are obtained using LC-BLYP/cc-pVTZ calculations. The CPCM model of water is considered for the solvent model.

Fig. 3. Images of the molecular orbitals depicting the main transitions of the three lowest-lying singlet excitations of the single OH-terminated SiPc for the monomer and π-stacking dimer. The transitions of the excitations are determined using spin-flip LC-TDBLYP/cc-pVTZ calculations, while the molecular orbital images are obtained using LC-BLYP/cc-pVTZ calculations. The CPCM model of water is considered for the solvent model.

Fig. 4. Images of the molecular orbitals illustrating the main transitions of the three lowest-lying singlet excitations of the double OH-terminated SiPc for the monomer and π-stacking dimer. The transitions of the excitations are determined using spin-flip LC-TDBLYP/cc-pVTZ calculations, while the molecular orbital images are obtained using LC-BLYP/cc-pVTZ calculations. The CPCM model of water is considered for the solvent model.

Fig. 5. Schematic diagram depicting the triplet generation mechanism of SiPc.

References

(1) Mitra, K.; Hartman, M. C. T. Silicon phthalocyanines: synthesis and resurgent applications. *Org. Biomol. Chem.* **2021**, *19*, 1168–1190.

(2) Lessard, B. H. The Rise of Silicon Phthalocyanine: From Organic Photovoltaics to Organic Thin Film Transistors. *ACS Appl. Mater. Interfaces* **2021**, *13*, 31321–31330.

(3) Lessard, B. H.; White, R. T.; AL-Amar, M.; Plint, T.; Castrucci, J. S.; Josey, D. S.; Lu, Z.-H.; Bender, T. P. Assessing the Potential Roles of Silicon and Germanium Phthalocyanines in Planar Heterojunction Organic Photovoltaic Devices and How Pentafluoro Phenoxylation Can Enhance π-π Interactions and Device Performance. *ACS Appl. Mater. Interfaces* **2015**, *7*, 5076–5088.

(4) Ke, L.; Gasparini, N.; Min, J.; Zhang, H.; Adam, M.; Rechberger, S.; Forberich, K.; Zhang, C.; Spiecker, E.; Tykwinski, R. R. et al. Panchromatic ternary/quaternary polymer/fullerene BHJ solar cells based on novel silicon naphthalocyanine and silicon phthalocyanine dye sensitizers. *J. Mater. Chem. A* **2017**, *5*, 2550–2562.

(5) Vebber, M. C.; Rice, N. A.; Brusso, J. L.; Lessard, B. H. Thermodynamic Property-Performance Relationships in Silicon Phthalocyanine-Based Organic Photovoltaics. *ACS Appl. Mater. Interfaces* **2022**, *5*, 3426–3435.

(6) Zysman-Colman, E.; Ghosh, S. S.; Xie, G.; Varghese, S.; Chowdhury, M.; Sharma, N.; Cordes, D. B.; Slawin, A. M. Z.; Samuel, I. D. W. Solution-Processable Silicon Phthalocyanines in Electroluminescent and Photovoltaic Devices. *ACS Appl. Mater. Interfaces* **2016**, *8*, 9247–9253.

(7) Pearson, A. J.; Plint, T.; Jones, S. T. E.; Lessard, B. H.; Credgington, D.; Bender, T. P.; Greenham, N. C. Silicon phthalocyanines as dopant red emitters for efficient solution processed OLEDs. *J. Mater. Chem. C* **2017**, *5*, 12688–12698.

(8) Grant, T. M.; Dindault, C.; Rice, N. A.; Swaraj, S.; Lessard, B. H. Synthetically facile organic solar cells with >4% efficiency using P3HT and a silicon phthalocyanine non-fullerene acceptor. *Mater. Adv.* **2021**, *2*, 2594–2599.

(9) Mitsunaga, M.; Ogawa, M.; Kosaka, N.; Rosenblum, L. T.; Choyke, P. L.; Kobayashi, H. Cancer cell-selective in vivo near infrared photoimmunotherapy targeting specific membrane molecules. *Nature Med.* **2011**, *17*, 1685–1691.

(10) Oddos-Marcel, L.; Madeore, F.; Bock, A.; Neher, D.; Ferencz, A.; Rengel, H.; Wegner, G.; Kryschi, C.; Trommsdorff, H. P. Electronic States and Relaxation Dynamics of Silicon Phthalocyanine Dimers. *J. Phys. Chem.* **1996**, *100*, 11850–11856.

(11) Hush, N. S.; Woolsey, I. S. The electronic absorption spectra of phthalocyanine monomers and dimers. *Mol. Phys.* **1971**, *21*, 465–474.

(12) Tsuneda, T.; Taketsugu, T. Singlet fission initiating organic photosensitizations. *Under review* **2023**, *12*, 19714–19722.

(13) Tsuneda, T.; Taketsugu, T. Singlet fission initiating triplet generations of BODIPY derivatives through π-stacking: a theoretical study. *Sci. Rep.* **2022**, *12*, 19714–19722.

(14) Smith, M. B.; Michl, J. Singlet Fission. *Chem. Rev.* **2010**, *110*, 6891–6936.

(15) Weiss, L. R.; Bayliss, S. L.; Kraffert, F.; Thorley, K. J.; Anthony, J. E.; Bittl, R.; Friend, R. H.; Rao, A.; Greenham, N. C.; Behrends, J. Strongly exchange-coupled triplet pairs in an organic semiconductor. *Nat. Phys.* **2017**, *13*, 176–181.

(16) Tayebjee, M. J. Y.; Sanders, S. N.; Kumarasamy, E.; Campos, L. M.; Sfeir, M. Y.; McCamey, D. R. Quintet multiexciton dynamics in singlet fission. *Nat. Phys.* **2017**, *13*, 182–188.

(17) Matsuda, S.; Oyama, S.; Kobori, Y. Electron spin polarization generated by transport

of singlet and quintet multiexcitons to spincorrelated triplet pairs during singlet fissions. *Chem. Sci.* **2020**, *11*, 2934–2942.

(18) Ito, S.; Nagami, T.; Nakano, M. Molecular design for efficient singlet fission. *J. Photochem. Photobio. C: Photochem. Rev.* **2018**, *34*, 85–120.

(19) Korovina, N. V.; Das, S.; Nett, Z.; Feng, X.; Joy, J.; Haiges, R.; Krylov, A. I.; Bradforth, S. E.; Thompson, M. E. Singlet Fission in a Covalently Linked Cofacial Alkynyltetracene Dimer. *J. Am. Chem. Soc.* **2016**, *138*, 617–627.

(20) Walker, B. J.; Musser, A. J.; Beljonne, D.; Friend, R. H. Singlet exciton fission in solution. *Nature Chem.* **2013**, *5*, 1019–1024.

(21) Sato, K.; Ando, K.; Okuyama, S.; Moriguchi, S.; Ogura, T.; Totoki, S.; Hanaoka, H.; Nagaya, T.; Kokawa, R.; Takakura, H. et al. Photoinduced Ligand Release from a Silicon Phthalocyanine Dye Conjugated with Monoclonal Antibodies: A Mechanism of Cancer Cell Cytotoxicity after Near-Infrared Photoimmunotherapy. *ACS Cent. Sci.* **2018**, *4*, 1559–1569.

(22) Postils, V.; Ruiperez, F.; Casanova, D. Mild Open-Shell Character of BODIPY and Its Impact on Singlet and Triplet Excitation Energies. *J. Chem. Theory Comput.* **2021**, *17*, 5825–5838.

(23) Krylov, A. I. Size-consistent wave functions for bond-breaking: The equation-of-motion spin-flip model. *Chem. Phys. Lett.* **2001**, *338*, 375–384.

(24) Shao, Y.; Head-Gordon, M.; Krylov, A. I. The spin-flip approach within time-dependent density functional theory: Theory and applications to diradicals. *J. Chem. Phys.* **2003**, *118*, 4807–4818.

(25) Iikura, H.; Tsuneda, T.; Yanai, T.; Hirao, K. A long-range correction scheme for

generalized-gradient-approximation exchange functionals. *J. Chem. Phys.* **2001**, *115*, 3540–3544.

(26) Tsuneda, T.; Hirao, K. Long-range correction for density functional theory. *WIREs Comput. Mol. Sci.* **2014**, *4*, 375–390.

(27) Becke, A. D. Density-functional exchange-energy approximation with correct asymptotic behavior. *Phys. Rev. A* **1988**, *38*, 3098–3100.

(28) Lee, C.; Yang, W.; Parr, R. G. Development of the Colle-Salvetti correlation-energy formula into a functional of the electron density. *Phys. Rev. B* **1988**, *37*, 785–789.

(29) Kendall, R. A.; Dunning Jr., T. H.; Harrison, R. J. Electron affinities of the first-row atoms revisited. Systematic basis sets and wave functions. *J. Chem. Phys.* **1992**, *96*, 6796–6806.

(30) Tomasi, J.; Mennucci, B.; Cammi, R. Quantum mechanical continuum solvation models. *Chem. Rev.* **2005**, *105*, 2999–3093.

(31) Tsuneda, T.; Singh, R. K.; Nakata, A. Relationship Between Orbital Energy Gaps and Excitation Energies for Long-Chain Systems. *J. Comput. Chem.* **2016**, *37*, 1451–1462.

(32) Tsuneda, T.; Singh, R. K.; Nakata, A. On Low-Lying Excited States of Extended Nanographenes. *J. Comput. Chem.* **2017**, *38*, 2020–2029.

(33) Frisch, M. J.; Trucks, G. W.; Schlegel, H. B.; Scuseria, G. E.; Robb, M. A.; Cheeseman, J. R.; Scalmani, G.; Barone, V.; Petersson, G. A.; Nakatsuji, H. et al. Gaussian 16 Revision A.03. 2016; Gaussian Inc. Wallingford CT.

(34) Schmidt, M. W.; Baldridge, K. K.; Boatz, J. A.; Elbert, S. T.; Gordon, M. S.; Jensen, J. H.; Koseki, S.; Matsunaga, N.; Nguyen, K. A.; Su, S. et al. General atomic and molecular electronic structure system. *J. Comput. Chem.* **1993**, *14*, 1347–1363.

(35) Kobayashi, M.; Harada, M.; Takakura, H.; Ando, K.; Goto, Y.; Tsuneda, T.; Ogawa, M.; Taketsugu, T. Theoretical and Experimental Studies on the Near-Infrared Photoreaction Mechanism of a Silicon Phthalocyanine Photoimmunotherapy Dye: Photoinduced Hydrolysis by Radical Anion Generation. *ChemPlusChem* **2020**, *85*, 1–6.

(36) El-Sayed, M. A. The Radiationless Processes Involving Change of Multiplicity in the Diazenes. *J. Chem. Phys.* **1962**, *36*, 573–574.

(37) Yabumoto, S.; Sato, S.; Hamaguchi, H. Vibrational and electronic infrared absorption spectra of benzophenone in the lowest excited triplet state. *Chem. Phys. Lett.* **2005**, *416*, 100–103.

(38) Takakura, H.; Goto, Y.; Kitamura, A.; Yoshihara, T.; Tobita, S.; Kinjo, M.; Ogawa, M. Analysis of the triplet-state kinetics of a photosensitizer for photoimmunotherapy by fluorescence correlation spectroscopy. *J. Photochem. Photobio. A: Chemistry* **2021**, *408*, 113094(1–6).